Interface Sensor Based on Computer Vision: Fine Tuning Using a Fluidized Bed

Jesus Guardiola
Dept. of Chemical Engineering, Universidad de Alcalá, Alcalá de Henares, Madrid 28871, Spain

Jose M. Aragón
Faculty of Chemistry, Dept. of Chemical Engineering, University Complutense de Madrid, Madrid 28040, Spain

Guadalupe Ramos, Rosario Elvira, and Daniel Martín
Dept. of Chemical Engineering, Universidad de Alcalá, Alcalá de Henares, Madrid 28871, Spain

DOI 10.1002/aic.13756
Published online February 17, 2012 in Wiley Online Library (wileyonlinelibrary.com).

The fine tuning of a sensor designed to locate interfaces using a two-dimensional gas–solid fluidized bed (FB) as reference is described. The sensor works through computer vision and consists of a charge coupled device camera that is placed alongside the bed and, as the human eye would do, first establishes a straight segment of the bed's top surface to define the phase boundary and then through pattern recognition continuously scans the interface in search of a similar pattern. The field of view is 582 × 752 pixels^2. The experimentally measured Pixel size is 216 × 208 μm^2. The device allows for experimentally obtaining the position of the probe with a resolution of ± 0.01 pixels at 25 Hz. We also describe its use to measure the height of the FB and observe a linear relationship with fluidization velocity. © 2012 American Institute of Chemical Engineers *AIChE J,* 58: 3645–3652, 2012
Keywords: computer vision, fluidized bed, interface, pattern recognition, sensor

Introduction

Macroscopic type interfaces are common in technological operations and processes. The term macroscopic is used here to define interfaces at which the liquid or gas is not subdivided as occurs with the level reached by liquids and solid–gas fluidized beds (FBs), but it excludes the interfaces produced when solid particles, liquid drops, or gas bubbles are immersed in fluids. In this article, we only refer to these macroscopic interfaces. The economic importance of such interfaces is considerable with applications such as stocktaking of the contents of tanks, monitoring sedimentation in wastewater treatment plants, and determining the volume occupied by a fluid catalytic cracking unit when refining crude oil.

Macroscopic interfaces can occupy a vertical or horizontal spatial position but most frequently they occur in a horizontal plane and can be detected by level sensors. Specific level sensors exist for granular materials or liquids, and some are common to both. These sensors are used to detect both point and continuous levels. When electrical or electromagnetic energy is put into the system, a sensor picks up the disturbance caused by the discontinuity of the interface itself. This causes a change in the transmission of visible or ultraviolet light, radiofrequency energy, or variations in the electrical properties of the medium. In many devices, the transmitter and the receiver are linked to form the sensor. Among the sensors, optical fibers are most widely used to monitor liquid levels, and several types exist such as side-polished fiber Bragg gratings,[1] intensity modulated fibers,[2] and the Fabry–Perot interferometer.[3] Also for liquids, a torsional acoustic waveguide sensor[4] may be used or an ultrasonic sensor[5] for petrochemical tanks. Capacitors[6,7] are also used, the latest models being grounded. Changes in electrical resistance are measured using a constant current source.[8] Finally, an original way of measuring the level of liquid in a tank is to find the equation of the plane of the liquid–gas interface from its intersection with three laser beams; the plane can then be pinpointed with one or two cameras.[9]

With some adjustments, the above techniques can also be used for granular solids in hoppers or FBs. Measuring grain in silos is complex because of the flatness of the grain interface and dust generated, and the devices used are also complex.[10] For FBs, probably the most accurate method is the use of pressure measurements. To do this, a variety of probes are placed on the bed, and the height at which the pressure is equal to that of the freeboard is determined by extrapolation.[11] Llop et al.,[12] for example, used three pressure probes to assess the effects of pressure and temperature on bed expansion. Crandfield and Geldart[13] captured cinephoto images of the upper surface to calculate the expansion of coarse-particle beds. A similar technique based on the use of current image analysis tools was described by Busciglio et al.,[14] in which the area corresponding to the bed was

Correspondence concerning this article should be addressed to J. Guardiola at jesus.guardiola@uah.es.

measured in video images captured with a charge coupled device (CCD). Watano et al.[15] used an ultrasonic displacement sensor linked to a CCD video camera.

Electrical capacitance tomography has been used to calculate the porosity of a given bed volume. However, extrapolating the value of porosity to the whole bed produces erroneous results, as for this property, there are considerable differences between different regions of the bed, for example, jets that are close to the distributor as opposed to the dense phase in the upper region of the bed. Delmon et al.[16] described a capacitor model fitted to a cylindrical column consisting of two metal plates; thus, its resolution will be lower than that of the devices used by other authors, which typically have 8 or 12 plates. A wireless device also exists with a passive inductor–capacitor circuit designed for granular-type substances as well as liquid.[17] It should be noted that solid objects such as rods, floats, and rotating paddles are required in most of the sensors mentioned.

In general, sensors for liquid interfaces show a higher performance than those used for granular solids. Thus, Lu et al.[3] reported a resolving power of about 0.4 mm and a precision of 1 mm over a range of 2.3 m of water column (pressure), and Sheng et al.[18] reported a sensitivity of 1.526 $\times$ 10^{-5} cm^{-1} of water level. In addition, an accuracy of 2 mm over a full scale of 3.5 m water,[19] a resolution better than 0.10 mm for a measuring time of 20 ms,[7] and a magnetostriction sensor with a resolution of 0.10 mm[20] have been described. An original method is to apply a subpixel polynomial interpolation algorithm for the liquid edge positioning.[21] For granular solids, it is rather more difficult to find information. Thus, Al Zahrani and Daous[22] report a sampling rate of 10^4 samples/s with an accuracy of 0.01 psi, though this is an indirect method through pressure signals. The sampling frequency of the measures varies widely among authors.

Finally, despite numerous high-performance instruments on the market, many of these systems rely on probes, which make them intrusive techniques, and they also need more or less complex electronics. Sometimes, there are also physical problems of space to accommodate the equipment's components and problems arising from distortion of the energy beam due to the undulating nature of the surface; for example, the waves on the surface of a liquid.

Before such devices were introduced, the level of an interface was detected visually through comparison with a graduated scale, and accuracy and resolution were low. The rationale for the technique proposed here is that computer vision can today imitate an observer and improve on the limitations of the human eye. The technique described is the use of a CCD camera to capture a two-phase system. An interface segment representative of its position is chosen, and its height coordinates are measured; the length of the reference segment is decided on previously. Therefore, it is, a procedure of pattern recognition. Herein, we describe its application to a two-dimensional (2-D) gas–solid FB operating under laboratory pressure and temperature conditions.

The most important advantage of the technique is that it is nonintrusive. Its main drawback is that the CCD has to visualize the interface, so that, in principle, its applications would be limited to transparent fluidized systems. However, this does not substantially limit the methods use. Thus, it can be applied to industrial scale processes such as drying of solids, and more particularly to foodstuffs, granulation and coating of pharmaceutical products, biofluidization, and culture of microorganisms, which is conducted at about 28–30°C. The technique can also be used to measure liquid levels in tanks at near atmospheric pressure, and even when processes are carried out at high P or T, by installing a peephole in the wall of the container (as used in glass-refining furnaces).

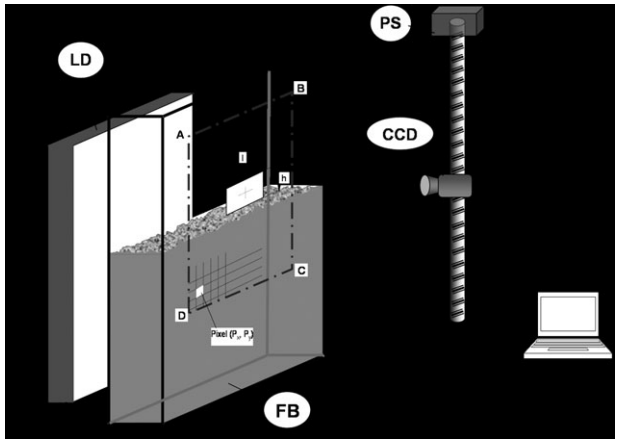

Figure 1. Diagram illustrating the device setup.

Equipment and Operating Procedure

The experimental setup consists of a 2-D solid–gas FB and a computer vision system (Figure 1). The fluidized material (glass ballotini of particle size $420 < d_p < 500$ μm) is contained between two sheets of methyl methacrylate measuring 1.0 m (height) $\times$ 0.2 m (width) $\times$ 0.009 m (depth). The system is fed with air at 18°C through a distributor, which is a stainless steel plate perforated with 0.3-mm holes placed 5 mm apart in a triangular arrangement. The fluidization gas moisture of 60% is obtained by bubbling air through water and measured with a hygrometer Testo 635; the material does not acquire electrostatic charge at this moisture level.

The computer vision system consists of a CCD camera, a positioning system (PS) to slide the camera up and down, a backlighting device (LD), and software to manage the image capturing process. The CCD camera used was a Sony XC-75CE with a sensitive element of 582 pixels (horizontal dimension) $\times$ 752 pixels (vertical dimension) that is positioned 0.36 m away from the bed and yields grayscale images. The pixel size of this sensitive element is 8.6 μm (width) $\times$ 8.3 μm (height). The field of view of the camera on the lateral surface of the FB is displayed in the figure (line ABCD). The size of the view field and the size of its unit of measure depend on the distance CCD-bed. Hereafter, this unit of measure is called Pixel (indicated in Figure 1); its dimensions are P_x μm (width) $\times$ P_y μm (height) and these are experimentally obtained. The camera captures 25 image/s, and the images are binarized at a threshold that can be selected manually or automatically. The CCD is connected to a PC that regulates its operation using customized software.

The PS is an automated RoboCylinder ERC-SA6, which includes a motor, and is connected to a PC. The PS can move the camera at a velocity of $0.001 \leq v_p \leq 0.100$ m/s. The device can be programmed to move the camera to eight

locations. Its stroke is 0.45 m and resolution is $\pm$ 3 $\times$ 10^{-5} m.

The LD is a 2-D strobe source of light placed 0.20 m behind the bed whose operation is synchronized with that of the CCD.

The software controls the CCD and PS. Its objective is that the vision system checks the FB/air interface, that is, it laterally inspects the upper surface of the bed, finds the best horizontal segment, and records its position. Given the capture velocity of the CCD, the position of the segment is sampled at a frequency of 25 Hz.

A rectangular pattern can be established in two steps by the software:

1. Its dimensions (width $\times$ height, $w \times h$) are set and automatically positioned and its outline is visible in the center of the view field as a frame or window (Figure 1).

2. It is confirmed as a template, that is, the characteristics of the image within these limits are accepted and recorded. Thus, for example, by moving the camera, the pattern can be positioned, so that it is horizontally cut by the packed bed surface. The confirmation step includes binarizing the area, which is, therefore, split into two regions, the upper region corresponding to the freeboard comprised white Pixels and the lower region corresponding to the solid phase of black Pixels.

Methods of digital image analysis such as our system use a pattern. For instance, biometric identification systems such as facial and fingerprint recognition are well known. Our system is simpler, as a grayscale area is split only into two regions. The aforementioned creation of a pattern can be used as a tool to measure the height of the packed bed. This is conducted as follows: after completing the first step, as the lines of the rectangle that define the reference pattern are displayed on the monitor, the CCD is moved with the PS in manual mode to align one of its two horizontal lines (e.g., the upper limit of the window) with the bed's skyline and its position is read; next, the operation is repeated with the other horizontal line (e.g., the lower limit of the window). The fixed bed height is then given by the average of both measures. The resolutions of the position coordinates of the reference pattern and the bed height measures are $\pm$ 3$\cdot\times$ 10^{-5} m, the same as the resolution of the PS.

Operating procedure

The FB behaves like a boiling liquid such that an observer looking flush across the top surface will see some flat regions and other irregular regions where bubbles burst. Thus, a horizontal line through the flat regions will give the height of the boiling liquid. The system is based on this model and operates in four steps:

1. A horizontal surface pattern is created, that is, a straight fragment of interface that is not modified by exploding bubbles. To simplify the following operations, the pattern is rectangular ($w \times h$) and includes the segment of horizontal line mentioned.

2. The bed is fluidized, and the camera is moved manually to a position where the FB–air interface is located within its field of vision. The camera remains motionless at this position throughout the experiment.

3. By means of the software, a small region within the field of view is activated. This region of interest is of the same shape and size as the pattern, and it is able move freely within the image field and it is constantly tracking the area that best matches the pattern. This is termed the sensing region and plays the role of the probe in most sensors. The position coordinates of this sensing region and pattern matching are read and recorded to 25 Hz, respectively, x, y, and pm (Figure 2a–c).

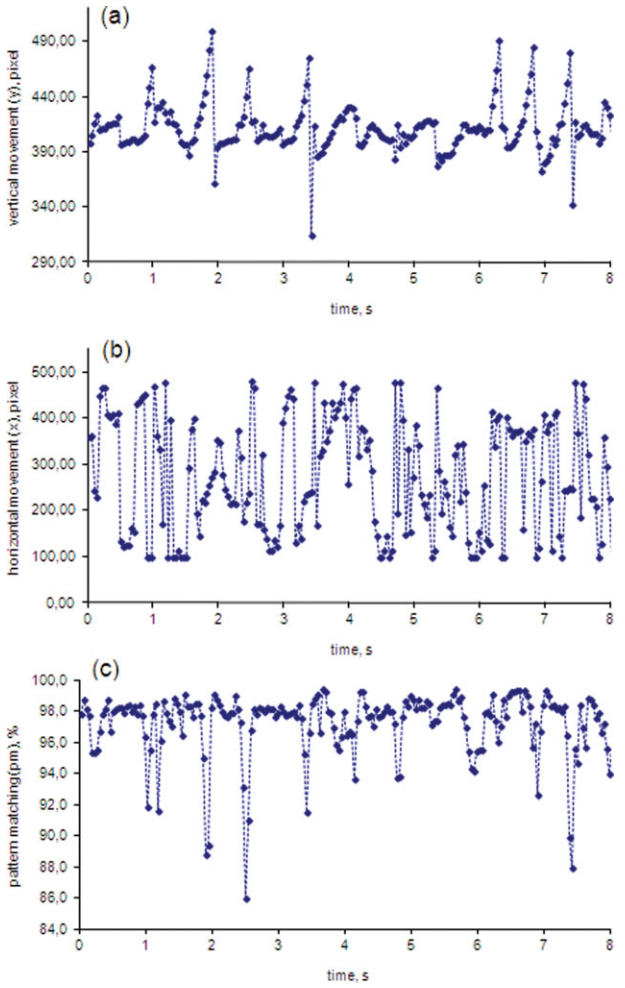

Figure 2. Results obtained for the movement of the sensing region.

(a) Vertical movement; (b) horizontal movement; and (c) pattern matching. [Color figure can be viewed in the online issue, which is available at wileyonlinelibrary.com.]

The resolution of the position coordinates of the sensing region is $\pm$ 0.01 pixels. This is because the device first positions the sensing region to match the maximum number of pixels and then calculates the mass center corresponding to all pixels belonging to the interface and included in the pattern. The aforementioned resolution and frequency were experimentally verified by a horizontal mark made on the fluidization column and taking measures over 28.952 s (724 images). The resulting values, taking as reference the PC clock and the reading of the mark, were 25.007 Hz and average height = 383.51 mm with standard deviation = 0.08 mm.

4. By disabling the sensing region, the run can be terminated by the operator.

One way to prepare the pattern during the first step could be to record a FB image, place this printed image in the field of view of the camera, and make the camera capture a horizontal linear segment. However, we prefer to directly capture the image of the glass ballotini-packed bed to be fluidized in the experiment. The error is negligible, as the histograms

Table 1. Experimental Conditions used to Examine the Effects of Sensor Geometry on the Measurements Obtained

Width (pixels)	Height (pixels)	Surface (pixels)	Number of Runs	Time per Run (s)
$41 \leq w \leq 544$	$544 \geq h \geq 41$	Always $w \times h = 22{,}304$	13	60
$27 \leq w \leq 544$	$544 \geq h \geq 27$	always w $\times$ $h = 14{,}688$		

FB/air and packed bed/air are similar and, consequently, the thresholds of binarization are also similar.

To identify the position and calculate the pm of the sensing region to which reference is made in Step 3 above, we have, on the one hand, an image of 582 $\times$ 752 pixels^2, and on the other hand, the sensing region (a rectangle, e.g., 275 $\times$ 81 pixels^2 in which the top 50% could be white and the bottom 50% could be black). The image is binarized resulting in a decomposed image of black and white Pixels. Next, the sensing region is activated. This means that the probe searches for a region of the same shape and size as the pattern in the image and also makes sure that the numbers of black and white Pixels and their distribution the most match with the pattern.

Results and Discussion

Communication with the vision system is achieved through pixel units, that is, the input of the pattern size and the output of the coordinates of the sensing region. Although according to the described installation and operating procedure, one might assume the measurement technique could simply involve calibrating Pixel size (P_x, P_y), for example, using horizontal and vertical marks on the fluidization column, this, however, would be insufficient to ensure the reproducibility of the measure. This is because the sensor system is designed to locate interfaces that are not well defined or fluctuate such as that of a FB. For instance, when applied to a FB, if the sensing region is large, it will not freely move across the interface and pattern matching will be low. The device's parameters are discussed below to confirm that they do not affect the measurement results.

Effects of sensing region geometry and area

As the sensing region is 2-D, tests were conducted keeping the surface area constant while varying the height to width ratio (h/w). The conditions used are indicated in Table 1. Figure 3 shows the variation in pm versus h/w for the given conditions. The results indicate that tall sensing regions offer greater agreement than flatter regions. Both variables (height and width) contribute to this behavior. Thus, when analyzed separately (Figure 4), both have a critical point beyond which the pm asymptotically approaches 100%. The change in the slope of pm versus h/w was used as the criterion to select the geometry of the sensing region. Thus, the data for $h \times w = 22{,}304$ in Figure 3 were fitted to two lines, and their intersection was calculated: $h/w = 0.290$ and pm = 97.20%. Therefore, for a sensing region of this size, the measurement technique cannot be used for $h/w \leq 0.290$ or, in other words, for $w \geq 275$ pixels and $h \leq 81$ pixels. The process was repeated for other sensing region sizes to give the results shown in Table 2 (In all cases, the point for $h/w \approx 0.5$ was excluded before fitting the data, as this point seemed to correspond to the transition region between the two behaviors). As height and width values (plotted in Figure 5) yielded a straight line, we can infer that for the sensing region sizes tested, the dimensions of the probe must fulfill the condition $h/w \geq 0.58$.

Another approach to examine the effects of the probe's dimensions would be to establish a minimum pm value: for example, in Figure 3 for $h \times w = 22{,}304$ when pm $\geq$ 97% the first experimental datum that satisfies this condition is pm = 97.18% and $h/w = 0.596$ (or $w = 193$ pixels and $h = 115$ pixels). The results for the areas tested provided in Table 3 and Figure 5 indicate that the condition is $h/w \geq 0.85$ regardless of the size of the pattern. In conclusion, under the conditions tested, the height/width ratio for the pattern has a lower limit but no upper limit.

Minimum sampling time to obtain a representative measure of a fluctuating interface

The position of the interface over time is given in Figure 2a. Once this series of data is completed, we will analyze the phenomenon, for example, using statistical tools or in the frequency domain or phase space. However, as the values obtained are instantaneous, it will be useful to know the minimum number of points needed to obtain the average value that represents the location of the interface, and whether there is any relationship between the characteristics of the probe, the minimum number of points mentioned

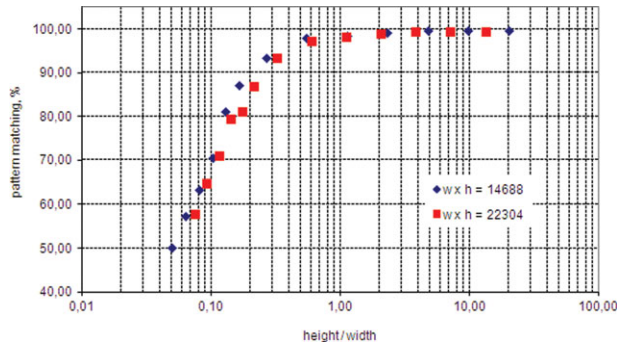

Figure 3. Variation in pattern matching with sensing region geometry.

Each point is the average of the data recorded over a run time of 60 s. [Color figure can be viewed in the online issue, which is available at wileyonlinelibrary.com.]

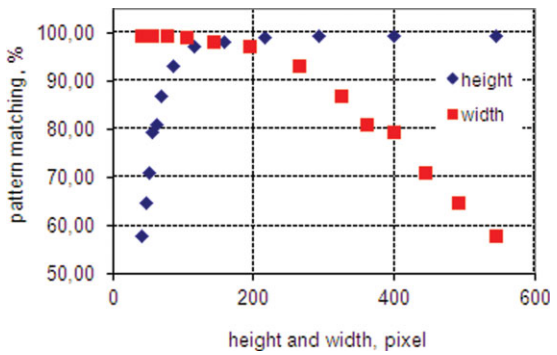

Figure 4. Effect of sensing region dimensions on pattern matching. $h \times w = 22{,}304$ pixels.

[Color figure can be viewed in the online issue, which is available at wileyonlinelibrary.com.]

Table 2. Intersections Between Lines Obtained in Experiments Similar to Those Indicated in Figure 3

	Upward Line		Horizontal Nearly Line		Intersection Point Both Lines		
$w \times h$	Slope	y-Intercept	Slope	y-Intercept	w	h	pm
10,880	79.77	149.15	1.06	98.47	219	50	97.79
14,688	71.92	143.29	1.15	98.54	251	59	97.81
18,496	64.08	132.73	1.69	98.09	258	72	97.16
22,304	64.52	131.48	1.65	98.08	275	81	97.20
26,112	63.38	129.49	1.90	98.09	291	90	97.12

above, and the values of both pm and the horizontal mobility of the probe while taking measurements.

To this, end tests were run in which 0.816 kg of glass ballotini were fluidized for 60 s. The relationship between the average pm and the number of points read (N) is shown in Figure 6a. One can observe that increasing the ratio h/w (i.e., the tallest pattern experiments) leads to an increase in pm, which is obtained with fewer measurements. When the height reached by the bed is analyzed (Figure 6b), a sampling time exists for which its average does not depend on the h/w relationship (about 8 s or 200 measurements). However, for probes in which $h/w = 0.596$ and $h/w = 13.268$, it can be observed that for 70–80 points, the difference between the average height and the long-term value is about 5–6 pixels, or given the value of P_y obtained later, only 1 mm. In principle, for the horizontal coordinate, x, the sensing region should be at any position on the bed surface line. However, some anomalous situations could exist such as bubble chains,[23] bubble flow patterns via preferential paths,[24] or when the bed is not completely vertical. Figure 6c shows that the average of the sensing region abscissa is fairly stable from about 600 points (24 s) confirming that in the long term, the probability that the probe occupies any location of the interface is constant. It should be noted that these values are significantly greater than the temporal and spatial resolutions of the probe (25.007 Hz and standard deviation = 0.08 for height 383.51 mm).

Finally, the high accuracy of the bed height measurements indicate that in some circumstances the technique could help resolve current problems of obtaining experimental data to validate CFD techniques.[25]

Influence of the phase distributions in the reference pattern

The established pattern comprises areas corresponding to the bed and the air above the bed, for example, 50/50%. In addition, fluidized material, previously released by the bubbles as they burst, sometimes falls from the freeboard to the upper surface. This material has been previously released by the bubbles when they burst on the same surface. To check whether this falling material affects the sensing region, we varied the bed/pattern relationship, $S_{b/p}$. The resultant effect of $S_{b/p}$ on pm is shown in Figure 7. The figure indicates reduced matching, as the difference between the two areas increases. Probably, the device has more difficulty in tracking the bed surface movement and finding the best match, when there is greater disproportion between the two areas.

Figure 8 shows the variation in bed height with $S_{b/p}$. We can observe that the measurement is nearly constant for $S_{b/p} \leq 0.4$, that is, when the area corresponding to the freeboard is greater than that corresponding to the FB. We, therefore, recommend the use of patterns whose bed/pattern proportions are slightly smaller than 0.5.

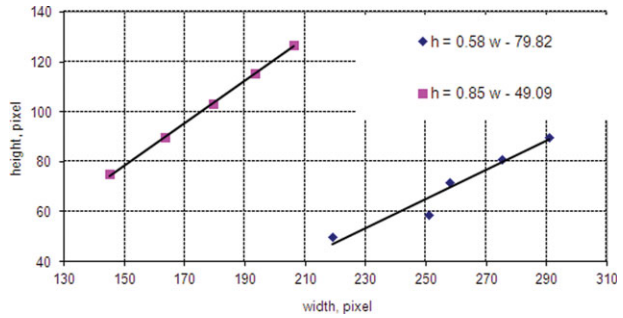

Figure 5. Influence of sensing region area on optimal geometry. ◆ Intersection points obtained in experiments similar to those indicated in Figure 3 and ■ pm ≥ 97.0%.

[Color figure can be viewed in the online issue, which is available at wileyonlinelibrary.com.]

Calculating the minimum field of view width and calibrating Pixel width

While making measurements, the sensing region moves along the top surface line so if this line is short the sensing region will have trouble finding good pattern matching. Accordingly, the behavior of a FB at $u_f = 0.526$ m/s using a sensing region $h = 157$ pixels and $w = 142$ pixels and horizontally limiting the camera's field of vision was examined. Figure 9 shows y values for four different widths of the field of vision. When the pm is low (less than a preset value) the sensing region moves to the position $y = 150$ pixels, which is a false value of the height and indicates that the measurement technique is not applicable in these conditions. Figure 10 shows that y is constant for $W \geq 0.108$ m; this is the shortest width across which the equipment can safely be operated. One way to shorten the minimum width of the field of view is to reduce w. Also by increasing the fluidization gas, interfaces become more irregular due to the presence of more bubbles, so w should be reduced or W should be increased to safely measure the interface.

In addition, the displacement limits of the sensing region for different widths of the visual field were used to calibrate Pixel width, P_x. To this end, the width of the visual field, W, was fixed, and measurements of the abscissa x for 15 min were obtained. Given that the probe constantly sweeps the interface with an equal probability of occupying any position, the maximum and minimum readings of x indicate the

Table 3. Geometry and Pattern Size When pm ≥ 97.0%

w (pixel)	h (pixel)	$w \times h$ (pixels^2)	pm (%)
145	75	10,880	97.72
164	90	14,688	97.95
179	103	18,496	97.16
193	115	22,304	97.18
206	127	26,112	97.12

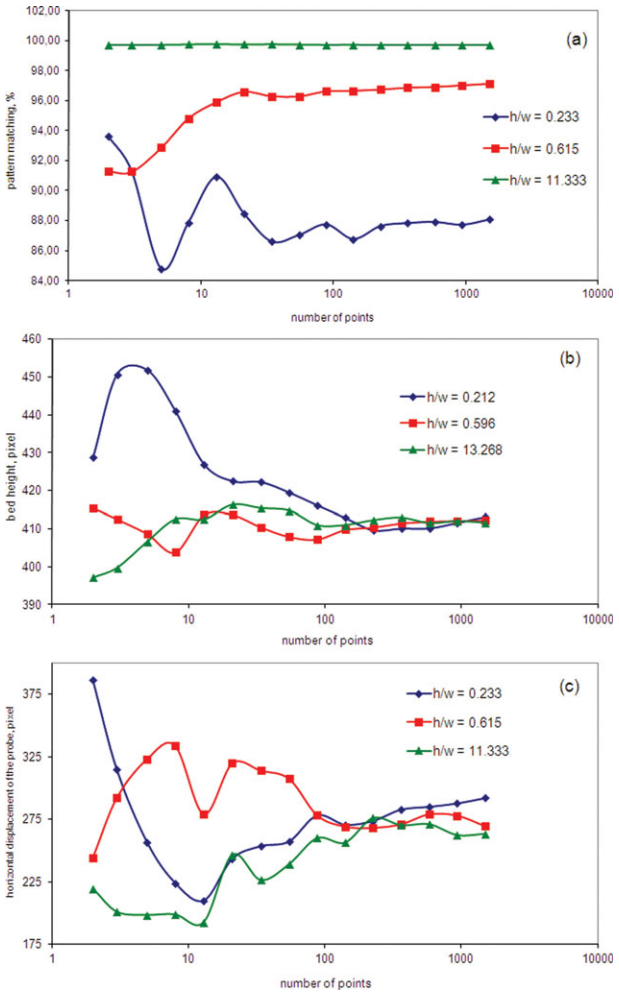

Figure 6. Minimum number of points yielding reproducible measurements.

(a) Matching between pattern and sensing region; (b) bed height; and (c) horizontal displacement of the sensor. [Color figure can be viewed in the online issue, which is available at wileyonlinelibrary.com.]

number of pixels falling within the width W. Figure 11 shows the minimum and maximum values obtained for several values of W, from which we calculated the range and calibration line. The slope of this line gives

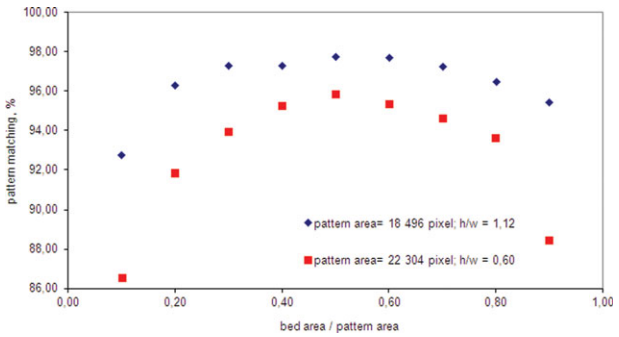

Figure 7. Optimal ratio between the pattern areas share. Run time for each point 60 s.

[Color figure can be viewed in the online issue, which is available at wileyonlinelibrary.com.]

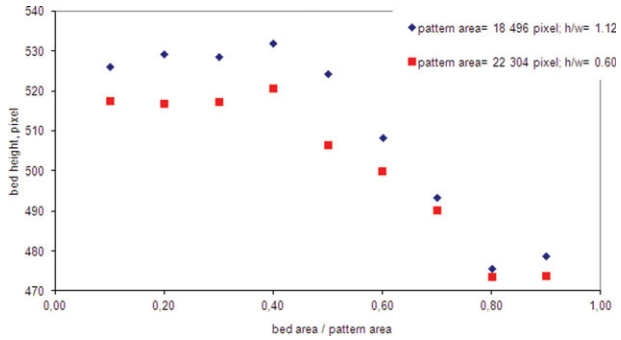

Figure 8. Effect of pattern area distributions on bed height measurements.

[Color figure can be viewed in the online issue, which is available at wileyonlinelibrary.com.]

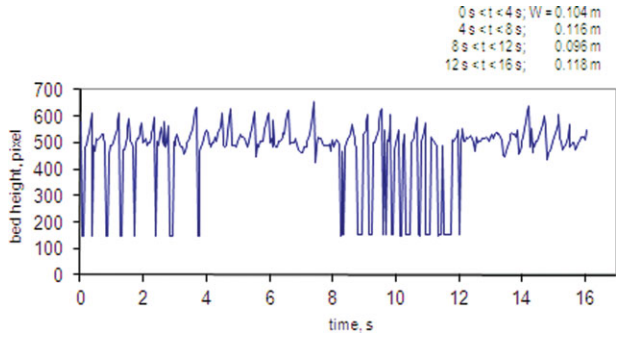

Figure 9. Field of view width and probe mobility: h = 157 pixels, w = 142 pixels; and u_f = 0.526 m/s.

[Color figure can be viewed in the online issue, which is available at wileyonlinelibrary.com.]

$$P_x = \frac{1}{4633}\text{m} = 216\ \mu\text{m} \tag{1}$$

for the camera-bed distance and focal length of the camera used.

Calibrating Pixel height

The vertical dimension of the Pixel (P_y) was calculated from the PS's scale. This was done by placing a horizontal mark on the fluidization column and taking measurements for various positions of the CCD. The displacement of the CCD with the PS can be programmed. Thus, we

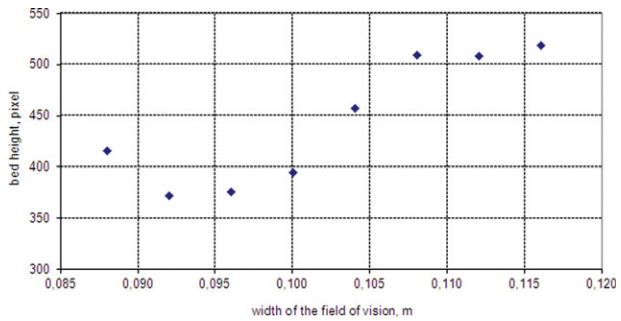

Figure 10. Effect of field of view width on bed height measurements: h = 157 pixels, w = 142 pixels; u_f = 0.526 m/s; and run time 60 s.

[Color figure can be viewed in the online issue, which is available at wileyonlinelibrary.com.]

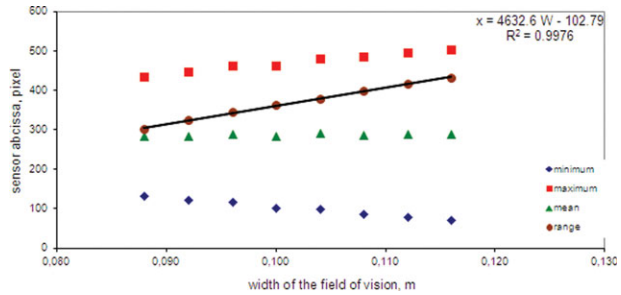

Figure 11. Calibrating Pixel width.

[Color figure can be viewed in the online issue, which is available at wileyonlinelibrary.com.]

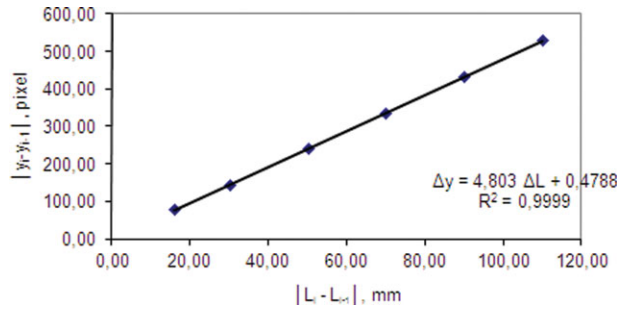

Figure 12. Calibrating Pixel height.

[Color figure can be viewed in the online issue, which is available at wileyonlinelibrary.com.]

programmed a cycle in which the center of the field of view of the camera was aligned with the mark and then the CCD was moved at a constant speed to several different positions. The packed bed itself was used as the mark, the readings of the mark for different positions of the CCD are shown in Figure 12, so that from the calibration line the following equivalence may be obtained

$$P_y = \frac{1}{4.803}\text{mm} = 208\ \mu\text{m} \tag{2}$$

Application to the relationship between gas flow and bed height

To assess the effects of gas flow, 0.816 kg of glass ballotini of 420–500 μm in size were fluidized with air at 18°C and gas flow was kept between 8.09×10^{-4} and 1.10×10^{-3} m^3/s.

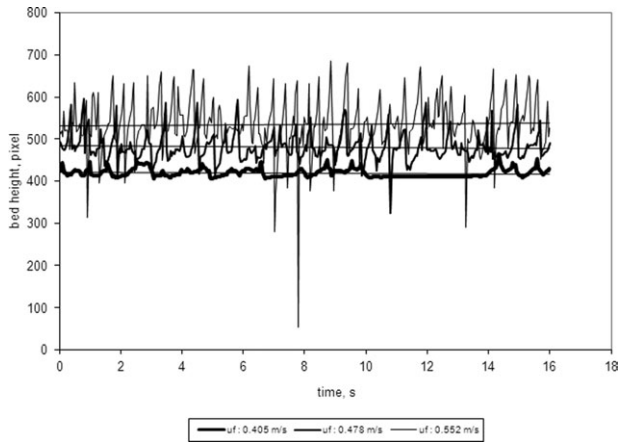

Figure 13. Changes in FB height over time.

Table 4. Bed Heights and pm for Several Gas Flows

Run	Fluidization Velocity (m/s)	Bed Height (pixel)		Pattern Matching (%)	
		y	σ_Y	pm	σ_{pm}
acp 347	0.405	421.69	12.30	98.55	1.41
acp 345	0.429	445.03	18.20	97.74	1.97
acp 342	0.454	464.12	24.39	96.80	2.70
acp 346	0.478	480.12	31.41	96.76	2.57
acp 343	0.503	500.70	42.79	96.32	3.26
acp 341	0.527	515.76	52.12	95.62	3.76
acp 344	0.552	532.00	61.22	95.54	3.76

Static bed height from the position of the distributor was 0.234 m. The results of three cases and lines of average values are presented in Figure 13. To clearly appreciate the phenomenon, a time of 16 s is shown in the figure, though each experiment lasted 120 s. The results of y and pm are included in Table 4, which shows that the standard deviation could probably be used as a measure of the global hydrodynamics of the bed. Figure 14 shows the fitting of the data.

Conclusions

Our results indicate that a computer vision-based sensor is suitable for locating the position of a macroscopic interface. The sensor proposed consists of a CCD camera and a PS that inspects the interface constantly searching for the flattest region. A rectangular sensing region moves within the camera's field of vision, which measures 582×752 pixels^2. The position coordinates of the sensing region (x and y) and the degree of matching to a given pattern are sampled at 25 Hz and obtained with a resolution of $\pm$ 0.01 pixels. Calibration of the system is simple, but its high performance depends on several key parameters that are need to be considered. When the upper surface of a 2-D FB was used as the interface to calibrate the sensor, we were able to determine that:

- The rectangular geometry of the sensing region affects pattern matching. Thus, its two dimensions have critical values and a minimum exists for its height and a maximum for its width. Both yield a minimum operation relationship, h/w.
- The minimum number of measures required to ensure that a measurement of the interface is reproducible is quite low. This figure depends on the pattern size and geometry used, although in general, the measure for pm is stable after 6 s of sampling and for y above 8 s. At 60 s, there is still some dispersion for x, as might be expected.
- When the area above the interface/area below the interface ratio is 50/50%, a maximum value of pm is obtained.

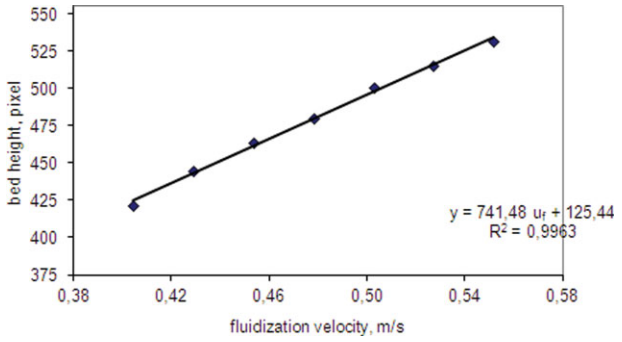

Figure 14. Effects of gas flow on FB height.

[Color figure can be viewed in the online issue, which is available at wileyonlinelibrary.com.]

However, considering that y is constant and peaks when the aforementioned ratio is $\geq$ 60/40%, we can conclude that the optimum measurement corresponds to a bed/pattern relationship of 40%.

- To avoid limiting the sensor's movements, the length of the interface must be at least 0.108 m.
- The dimensions of the Pixel depend on the configuration of the device. Here, its width was calculated by varying the width of the camera's field of vision and its height by displacing the camera and a Pixel size of 216 μm (width) $\times$ 208 μm (height) was obtained.
- Increasing gas flow causes an increase in the level of the bed and the standard deviation from the mean. In this case, the relationship between height and fluidization velocity is linear.

Acknowledgments

This study was supported by the Spanish Ministry of Research through Project CTQ2006-15525-C02-02. The hardware and software were designed in collaboration with Mr. JC Rubio from the Company Aida-Set, who is gratefully acknowledged for his dedicated work.

Notation

d_p = particle diameter, μm
h = height of the pattern and sensing region, pixel
L = locations to which the camera moves to gauge pixel height, mm
N = number of points sampled
P_x = horizontal dimension of the area unit of measure (Pixel), μm
P_y = vertical dimension of the area unit of measure (Pixel), μm
pm = pattern matching of the sensing region, %
$S_{b/p}$ = distribution of regions in the pattern: bed/pattern
u_f = fluidization velocity, m/s
v_p = velocity at which the PS moves the CCD, m/s
w = width of the pattern and sensing region, pixel
W = width of the field of vision, m
x = abscissa of the sensing region, pixel
y = ordinate of the sensing region, pixel

Greek letters

σ_y = standard deviation for the bed height
σ_{pm} = standard deviation for pattern matching

Literature Cited

1. Dong X, Zhao R. Detection of liquid-level variation using a side-polished fiber Bragg grating. *Opt Laser Technol*. 2010;42(1):214–218.
2. Linesh J, Sudeesh K, Radhakrishnan P, Nampoori V. Liquid level sensor using etched silica fiber. *Microwave Opt Technol Lett*. 2010;52(4):883–886.
3. Lu T, Li Z, Xia D, He K, Zhang G. Asymmetric Fabry–Perot fiber-optic pressure sensor for liquid-level measurement. *Rev Sci Instrum*. 2009;80(3):033104.
4. Spratt W, Vetelino J. Torsional acoustic waveguide sensor for temperature and liquid level. In: *2009 Joint Meeting of the European Frequency and Time Forum and the IEEE International Frequency Control Symposium*, New York: IEEE, *Vols. 1, 2*. 2009:850–854.
5. Sakharov V, Kuznetsov S, Zaitsev B, Kuznetsova I, Joshi S. Liquid level sensor using ultrasonic Lamb waves. *Ultrasonics*. 2003; 41(4):319–322.
6. Toth F, Meijer G, vanderLee M. A planar capacitive precision gauge for liquid-level and leakage detection. *IEEE Trans Instrum Meas*. 1997;46(2):644–646.
7. Reverter F, Li X, Meijer G. Liquid-level measurement system based on a remote grounded capacitive sensor. *Sens Actuators A*. 2007;138(1):1–8.
8. Zheng G, Zong H, Zhuan X, Luan J. Fast dynamic liquid level sensor based on liquid resistance. In: *2007 Africon*, New York: IEEE, *Vols. 1–3*. 2007:772–776.
9. Gaber C, Chetehouna K, Laurent H, Rosenberger C, Baron S. Optical sensor system using computer vision for the level measurement in oil tankers. In: *2008 IEEE International Symposium on Industrial Electronics,* New York: IEEE, *Vols. 1–5*. 2008:2148–2152.
10. Isiker H, Canbolat H. Concept for a novel grain level measurement method in silos. *Comput Electron Agric*. 2009;65(2):258–267.
11. Jovanovic G, Fitzgerald TJ, Catipovic NM. Expansion of fluidized beds of large particles: experiment and theory. In: *AIChE Annual Meeting*. Chicago, Illinois, 1980.
12. Llop MF, Casal J, Arnaldos J. Expansion of gas–solid fluidized beds at pressure and high temperature. *Powder Technol*. 2000;107:212–225.
13. Crandfield RR, Geldart D. Large particle fluidisation. *Chem Eng Sci*. 1974;29:935–947.
14. Busciglio A, Vella G, Micale G, Rizzuti L. Analysis of the bubbling behaviour of 2D gas solid fluidized beds. Part I. Digital image analysis technique. *Powder Technol*. 2008;140:398–413.
15. Watano S, Fukushima T, Miyanami K. The use of ultrasonic techniques for the measurement and control of bed height in tumbling fluidized-bed granulation. *Adv Powder Technol*. 1994;5:119–128.
16. Delmon G, Faure R, de Gasquet B, Giraud G, Clerc JP. Measurement of voidage in a fluidized bed using a capacitive sensor. *Powder Technol*. 1996;86:149–153.
17. Woodard S, Taylor B. A wireless fluid-level measurement technique. *Sens Actuators A*. 2007;137(2):268–278.
18. Sheng H, Liu W, Bor S, Chang H. Fiber-liquid-level sensor based on a fiber Bragg grating. *Jpn J Appl Phys*. 2008;47(4):2141–2143.
19. Lu T, Yang S. Extrinsic Fabry–Perot cavity optical fiber liquid-level sensor. *Appl Opt*. 2007;46(18):3682–3687.
20. Li Y, Sun L, Jin S. Development of magnetostriction sensor for online liquid level and density measurement. In: *WCICA 2006: Sixth World Congress on Intelligent Control and Automation, Vols. 1–12*, Conference Proceedings. New York: IEEE, 2006:5162–5166.
21. Zhao C, Chen Y. A new liquid level measuring system of standard metal tank based on sub-pixel edge detection. In: *2007 IEEE International Conference on Control and Automation,* New York: IEEE, *Vols. 1–7*. 2007:1327–1332.
22. Al Zahrani AA, Daous MA. Bed expansion and average bubble rise velocity in a gas–solid fluidized bed. *Powder Technol*. 1996;87:255–257.
23. Clift R, Grace JR. Coalescence of bubble chains in fluidized-beds. *Trans Instrum Chem Eng*. 1972;50:364–371.
24. Masson H. Solid circulation studies in a gas solid fluid bed. *Chem Eng Sci*. 1978;33:621–623.
25. Wang J, van der Hoef MA, Kuipers JAM. Why the two-fluid model fails to predict the bed expansion characteristics of Geldart A particles in gas-fluidized beds: a tentative answer. *Chem Eng Sci*. 2009;64:622–625.

Manuscript received Mar. 12, 2011, and revision received Jan. 8, 2012.